ULTRASOUND TOMOGRAPHY OF THE BREAST USING LINEAR ARRAYS

Pai-Chi Li and Sheng-Wen Huang

Department of Electrical Engineering, National Taiwan University, Taipei, Taiwan
paichi@cc.ee.ntu.edu.tw and f84048@ee.ntu.edu.tw

ABSTRACT

An approach for tomographic reconstructions of the sound velocity distribution and attenuation coefficient distribution in the breast using linear arrays is proposed. The time-of-flight and attenuation data are acquired by a linear array positioned at the top of a compressed breast and a metal plate is placed at the bottom as a reflector. The refraction effects on the attenuation data are compensated using a technique based on the angular spectrum method. A reconstruction algorithm based on a convex programming formulation and incorporating the segmentation information from the B-mode image is used. The experimental setup includes a phantom made of materials mimicking different tissues in the breast. Results show that obtaining the sound velocity distribution and attenuation coefficient distribution is feasible with the proposed algorithm under current B-mode imaging setup with linear arrays. Such an imaging method has the potential of enhancing the breast cancer detection.

1. INTRODUCTION

The sound velocity distribution and attenuation coefficient distribution in the breast can be used to complement B-mode ultrasound imaging in the detection of breast cancer. For example, the sound velocity is higher in cancerous tissue than in fat, and the attenuation coefficient is higher in cancerous tissue than in a cyst [1], [2]. Ultrasonic computed tomography has long been proposed for imaging the sound velocity and attenuation coefficient of the breast [3], but this has been hampered by the required imaging setup differing greatly from that used for B-mode imaging. Therefore, this study investigated a linear-array tomographic imaging setup enabling B-mode images, sound velocity distributions, and attenuation coefficient distributions to be acquired using a single setup. However, such a setup yields incomplete time-of-flight and attenuation data; hence, to improve the estimation accuracy, a reconstruction algorithm based on a convex programming formulation [4] and incorporating the segmentation information from the B-mode image was used. Furthermore, we developed a technique based on the angular spectrum method [5] that compensates for the refraction effects on the attenuation data. Performance of the approach was investigated using experimental data.

2. IMAGING SETUP

Consider the imaging setup shown in Fig. 1 [6]. The linear array has N_A channels and a metal plate is used for reflecting the acoustic wave. In addition to performing B-mode imaging, this setup is also capable of transmitting a pulse from a single channel in order to acquire a complete channel data set $\{e_{ij}(t)\}, 1 \le i, j \le N_A$, where $e_{ij}(t)$ is the signal received by channel j when only channel i transmits. Let $\{e_{O,ij}(t)\}$ be the complete channel data set with the object positioned between the array and the metal plate, and $\{e_{W,ij}(t)\}$ be the complete channel data set with the object replaced by water. With each $e_{(\circ),ij}(t)$, where $(\circ)$ denotes "O" (object) or "W" (water), a signal $a_{(\circ),ij}(t)$ corresponding specifically to the echo reflected from the bottom plate and the time-of-flight $t_{(\circ),ij}$ for the echo can be extracted.

Let $c(x,y)$ denote the sound velocity, $s(x,y) = c^{-1}(x,y)$ be the slowness, then the time of flight after geometrical delay compensation is

$$\Delta t_{ij} = t_{O,ij} - t_{W,ij} = \int_{L_{ij}} [s_O(x,y) - s_W]dl = \int_{L_{ij}} \Delta s(x,y)dl \,. \quad (1)$$

After discretizing $\Delta s(x,y)$,

$$\Delta t_{ij} = \sum_{n=1}^{N}\sum_{m=1}^{M} \Delta s(m,n) l_{ij}(m,n) = \mathbf{l}_{ij}^{\mathrm{T}} \Delta \mathbf{s}\,, \quad (2)$$

where $\mathbf{l}_{ij}$ and $\Delta\mathbf{s}$ are $MN \times 1$ column vectors, $(\mathbf{l}_{ij})_{(m-1)N+n} \equiv l_{ij}(m,n)$ is the contribution of grid point (m,n), $1 \le m \le M$, $1 \le n \le N$, and $(\Delta\mathbf{s})_{(m-1)N+n} \equiv \Delta s(m,n)$.

Based on the assumption of straight-line propagation path, $\mathbf{l}_{ij} = \mathbf{l}_{ji}$, and Δt_{ij} can be set to $(\Delta t_{ij} + \Delta t_{ji})/2$. The $N_A(N_A+1)/2$ equations in (2) can be put into the following matrix form:

$$\mathbf{L}\Delta\mathbf{s} = \Delta\mathbf{t}\,, \quad (3)$$

where $\Delta\mathbf{t} = \left[\Delta t_1 \quad \Delta t_2 \quad \cdots \quad \Delta t_{N_A(N_A+1)/2}\right]^{\mathrm{T}}$ and $\mathbf{L} = \left[\mathbf{l}_1 \quad \mathbf{l}_2 \quad \cdots \quad \mathbf{l}_{N_A(N_A+1)/2}\right]^{\mathrm{T}}$.

The equation for solving the attenuation coefficient

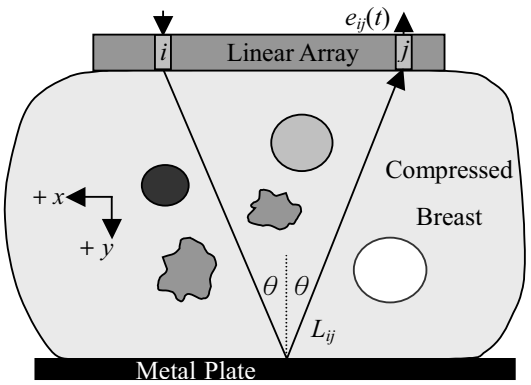

Fig. 1. Imaging setup.

distribution can be similarly derived. Let $A_{(\circ),ij}(f)$ denote the temporal spectrum of $a_{(\circ),ij}(t)$ and define

$$\Delta A_{ij}(f) = 20\log_{10}\left(\left|A_{\mathrm{W},ij}(f)\right|\right) - 20\log_{10}\left(\left|A_{\mathrm{O},ij}(f)\right|\right), \quad (4)$$

then

$$\Delta A_{ij}(f) = \int_{L_{ij}} \alpha_{\mathrm{dB,O}}(x,y;f)\,dl \cdot \quad (5)$$

In soft tissues, the attenuation coefficient is approximately a linear function of frequency over the frequency range considered here [3]. That is,

$$\alpha_{\mathrm{dB,O}}(x,y;f) \cong \alpha_{\mathrm{dB,O}}(x,y;f_0)\left|f/f_0\right|, \quad (6)$$

where f_0 is the frequency of interest. Define

$$\Delta\overline{A}_{ij}(f_0,\Delta f) = \frac{1}{\Delta f}\int_{f_0-\Delta f/2}^{f_0+\Delta f/2}\frac{f_0}{f}\Delta A_{ij}(f)\,df, \quad (7)$$

then

$$\Delta\overline{A}_{ij}(f_0,\Delta f) \cong \int_{L_{ij}} \alpha_{\mathrm{dB,O}}(x,y;f_0)\,dl \cong \mathbf{l}_{ij}^{\mathrm{T}}\boldsymbol{\alpha} \cdot \quad (8)$$

The $N_{\mathrm{A}}(N_{\mathrm{A}}+1)/2$ equations in (8) can be expressed in:

$$\mathbf{L}\boldsymbol{\alpha} = \Delta\mathbf{a}, \quad (9)$$

where the attenuation data $\Delta\mathbf{a}$ consists of $\Delta\overline{A}_{ij}(f_0,\Delta f)$.

3. CORRECTION OF THE ATTENUATION DATA

An acoustic wave propagating in an object with sound velocity inhomogeneities experiences both phase and amplitude distortion. Wavefront amplitude distortion affects $A_{\mathrm{O},ij}(f)$ and consequently also the estimation accuracy of the attenuation coefficient distribution. Here we developed a technique to compensate for such errors using the reconstructed sound velocity distribution. As illustrated in Fig. 2, consider an acoustic wave $W(x,y;f)$ propagating in the $+y$ direction in a medium with a sound velocity distribution of $c(x,y;f)$, a sound velocity of $c_0(f)$ in the background, and an attenuation coefficient of $\alpha_{0,\mathrm{dB}}(f)$ that is independent of the position. Given $W(x,0;f)$, $W(x,y_1;f)$ can be found by calculating $W(x,\mathrm{d}y;f)$, $W(x,2\mathrm{d}y;f)$, …, and $W(x,N_y\mathrm{d}y;f)$ sequentially with $N_y\mathrm{d}y = y_1$. Let the angular spectrum

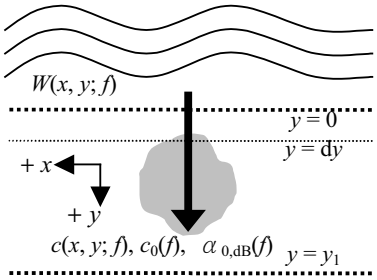

Fig. 2. Illustration of the technique for estimating the refraction effects.

of $W(x,y;f)$ be $\widetilde{W}(k_x;y,f)$ [5], i.e.,

$$W(x,y;f) = \frac{1}{2\pi}\int\widetilde{W}(k_x;y,f)\exp(jk_x x)\,dk_x, \quad (10)$$

then

$$W(x,q\mathrm{d}y+\mathrm{d}y;f) \cong \frac{h_q(x;f)}{2\pi}\int_{-2\pi f/c_0(f)}^{2\pi f/c_0(f)} H(k_x;\mathrm{d}y,f)\cdot \widetilde{W}(k_x;q\mathrm{d}y,f)\exp(jk_x x)\,dk_x, \quad (11)$$

where

$$h_q(x;f) = \exp\left\{j2\pi f\int_{q\mathrm{d}y}^{(q+1)\mathrm{d}y}\left[c^{-1}(x,y;f)-c_0^{-1}\right]dy\right\} \quad (12)$$

and

$$H = \exp\left[j\mathrm{d}y\sqrt{(2\pi f/c_0)^2-k_x^2}\right]10^{-\frac{\alpha_{0,\mathrm{dB}}(f)\mathrm{d}y}{20}\left\{\cos\left[\sin^{-1}(k_x c_0/f)\right]\right\}^{-1}}. \quad (13)$$

Based on the above discussion, an estimate $\hat{A}_{\mathrm{O},ij}(f)$ of $A_{\mathrm{O},ij}(f)$ taking the sound velocity inhomogeneities into account can be obtained by considering the metal plate as a mirror. An estimate of $A_{\mathrm{W},ij}(f)$, $\hat{A}_{\mathrm{W},ij}(f)$, can also be obtained. Define

$$\Delta\hat{A}_{ij}(f) = 20\log_{10}\left(\left|\hat{A}_{\mathrm{W},ij}(f)\right|\right) - 20\log_{10}\left(\left|\hat{A}_{\mathrm{O},ij}(f)\right|\right), \quad (14)$$

then a vector $\Delta\mathbf{a}'' = \mathbf{a} - \hat{\mathbf{a}}$, where $\hat{\mathbf{a}}$ consists of

$$\Delta\overline{\hat{A}}_{ij}(f_0,\Delta f) = \frac{1}{\Delta f}\int_{f_0-\Delta f/2}^{f_0+\Delta f/2}\frac{f_0}{f}\Delta\hat{A}_{ij}(f)\,df, \quad (15)$$

can be constructed, and the equation to be solved becomes

$$\mathbf{L}\boldsymbol{\alpha} = \Delta\mathbf{a}' \equiv \left(\Delta\mathbf{a}'' + \alpha_{0,\mathrm{dB}}(f_0)\mathbf{L}\mathbf{i}\right), \quad (16)$$

where $\mathbf{i}$ is an $MN\times 1$ vector whose elements all equal 1, and $\Delta\mathbf{a}' = \left[\Delta\overline{A}_1' \;\; \Delta\overline{A}_2' \;\; \ldots \;\; \Delta\overline{A}_{N_{\mathrm{A}}(N_{\mathrm{A}}+1)/2}'\right]^{\mathrm{T}}$ is the corrected attenuation data.

4. RECONSTRUCTION ALGORITHM

An algorithm based on a convex programming formulation for inconsistent problems [4] has been developed to solve (3) and (16). Two kinds of a priori knowledge are used. First, the sound velocity and attenuation coefficient are assumed to be in $[c_{\mathrm{lower}}, c_{\mathrm{upper}}]$ and $[\alpha_{\mathrm{dB,lower}}, \alpha_{\mathrm{dB,upper}}]$, respectively; therefore, $\Delta\mathbf{s}$ and $\boldsymbol{\alpha}$ must belong to

$$C_{\mathrm{velocity}} = \left\{\mathbf{x}\in\mathbf{R}^{MN} : x_l \in [c_{\mathrm{upper}}^{-1} - s_{\mathrm{W}}, c_{\mathrm{lower}}^{-1} - s_{\mathrm{W}}], \; 1\le l\le MN\right\} \quad (17)$$

and

$$C_{\text{attenuation}} = \left\{\mathbf{x} \in \mathbf{R}^{MN} : x_l \in [\alpha_{\text{dB,lower}}, \alpha_{\text{dB,upper}}], 1 \le l \le MN\right\}, \quad (18)$$

respectively. Second, segmentation information from the corresponding B-mode image is used. Consider a B-mode image in which an object contains an identified and segmented region of interest (ROI) surrounded by the background. Both $\Delta\mathbf{s}$ and $\boldsymbol{\alpha}$ must belong to the following set:

$$C_{\text{image}} = \left\{\mathbf{x} \in \mathbf{R}^{MN} : x_{b_1} = x_{b_2} = \cdots = x_{b_{N_b}}, x_{r_1} = x_{r_2} = \cdots = x_{r_{N_r}}, x_{br_i} \in F, 1 \le i \le N_{\text{br}}\right\} \quad (19)$$

where $I_{\text{b}} \equiv \{b_1, b_2, \ldots, b_{N_{\text{b}}}\}$ is the background index set, $I_{\text{r}} \equiv \{r_1, r_2, \ldots, r_{N_{\text{r}}}\}$ is the ROI index set, $I_{\text{br}} \equiv \{br_1, br_2, \ldots, br_{N_{\text{br}}}\}$ is the boundary index set, and F is the closed interval with x_{b_1} and x_{r_1} as its end points. Eq. (19) means that all the sound velocities (attenuation coefficients) in the background must be the same, and those in the ROI also must be the same. In addition, the sound velocities (attenuation coefficients) at the boundaries must fall between those of the background and the ROI. C_{image} can be defined similarly when the object contains more than one ROI.

Define

$$C_{\Delta t_i} = \left\{\mathbf{x} \in \mathbf{R}^{MN} : \mathbf{l}_i^{\mathrm{T}}\mathbf{x} = \Delta t_i\right\} \quad (20)$$

and

$$C_{\Delta A_i} = \left\{\mathbf{x} \in \mathbf{R}^{MN} : \mathbf{l}_i^{\mathrm{T}}\mathbf{x} = \Delta\overline{A}_i'(f_0, \Delta f)\right\}, \quad (21)$$

then a sound velocity (an attenuation coefficient) distribution $\mathbf{x} \in C_{\text{velocity}} \cap C_{\text{image}}$ ($C_{\text{attenuation}} \cap C_{\text{image}}$) minimizing the total amount of violation of the time-of-flight (attenuation) data in the mean-squared-error sense can be found by taking $\mathbf{x}$ as the limit of the sequence $\{\mathbf{x}_n\}$. $\mathbf{x}_0 \in C_{\text{velocity}} \cap C_{\text{image}}$ ($C_{\text{attenuation}} \cap C_{\text{image}}$) is an initial distribution, and

$$\mathbf{x}_{n+1} = \frac{1}{2}\left\{\mathbf{x}_n + P_{C_{\text{velocity}} \cap C_{\text{image}}}\left[\sum_{i=1}^{N_{\text{A}}(N_{\text{A}}+1)/2} \frac{P_{C_{\Delta t_i}}(\mathbf{x}_n)}{N_{\text{A}}(N_{\text{A}}+1)/2}\right]\right\}$$

$$\left(\mathbf{x}_{n+1} = \frac{1}{2}\mathbf{x}_n + \frac{1}{2}P_{C_{\text{attenuation}} \cap C_{\text{image}}}\left[\sum_{i=1}^{N_{\text{A}}(N_{\text{A}}+1)/2} \frac{P_{C_{\Delta A_i}}(\mathbf{x}_n)}{N_{\text{A}}(N_{\text{A}}+1)/2}\right]\right), \quad (22)$$

where $P_{C_{(\cdot)}}$ is the projector onto $C_{(\cdot)}$.

5. EXPERIMENTAL SETUP

A schematic of the experimental setup is shown in Fig. 3. The linear array (L6/128, STI, State College, PA) has $N_{\text{A}} = 128$ channels, an element pitch p of 0.3 mm, an elevation width of 5 mm, and an elevation focus of 25 mm. The array channels have a center frequency of 5.57 MHz and a –6 dB bandwidth of 4.10 MHz. A programmable digital array system (DiPhAS, Fraunhofer IBMT, St. Ingbert, Germany) [7] capable of transmitting a short pulse from any selected channel was used to acquire channel data, which were transferred to the computer for storage and further processing via a digital input/output card (PCI-7300A, ADLINK, Taipei County, Taiwan) on the computer. The transmitted pulse is a one-cycle square wave with a duration of 0.2 μs, and all data were sampled at 40 MHz with a resolution of 12 bits. For each transmit/receive combination, data corresponding to 16 consecutive firings were averaged off-line to increase the signal-to-noise ratio. The parameters of the different materials (mimicking different tissues in the breast) in the custom-made phantom (by Dr. Ernest Madsen, Department of Medical Physics, University of Wisconsin-Madison, WI) are listed in Table 1. The nine case illustrated in Fig. 3 were generated by moving the array along the *x*-axis.

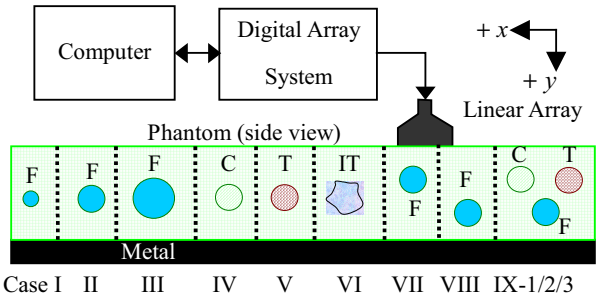

Fig. 3. The data-acquisition setup. The distance between the linear array and the metal plate is 36 mm. F, C, T, and IT stand for fat, cyst, high-attenuation tumor, and irregular tumor, respectively. In each case, the image object comprised a background (glandular tissue) and one or three ROIs. The dimensions of the ROIs in millimeters are 2, 4, 6, 4, 4, N/A, 4, 4, 4, 4, and 4 from the left to the right. All the centers of the ROIs (fats, cysts, and tumors) are in the same plane.

Table 1. Parameters of the materials (designed to mimic the listed tissues) used in the phantom (at 22° C).

Material	Sound velocity at 5 MHz (m/s)	Density (g/cm^3)	Attenuation coefficient at 5 MHz (dB/cm)	B-mode contrast (dB)
Glandular tissue	1522	1.03	2.74	reference
Fat	1464	0.94	2.21	–14
Cyst	1570	1.02	0.78	<–14
High-attenuation tumor	1547	1.10	7.36	–12
Irregular tumor	1553	1.07	4.26	–10

6. EXPERIMENTAL RESULTS

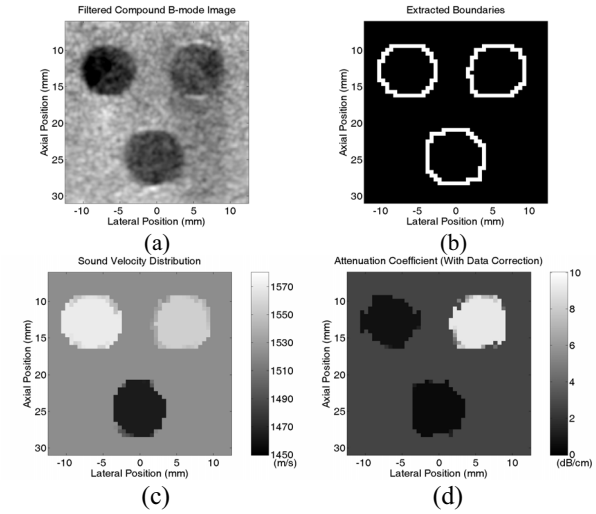

Fig. 4. Experimental results for Case IX.

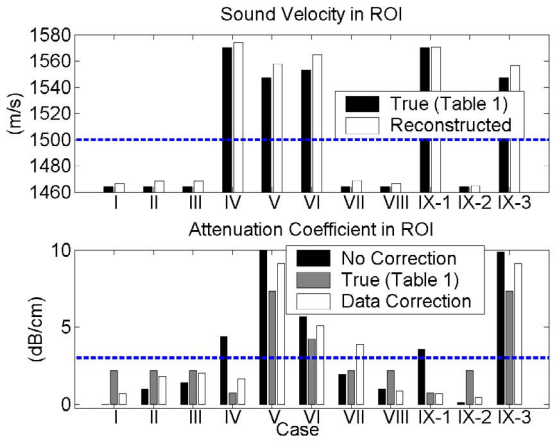

Fig. 5. Estimation results in ROIs.

Spatial compounding was performed to generate B-mode images with reduced speckle intensity variations. To further reduce the speckle variations, the compound B-mode image was low-pass filtered. A single threshold was applied to segment the filtered B-mode image and the result was used to derive the boundaries between the ROIs and the background in order to generate C_{image}.

Fig. 4 shows the results corresponding to different steps using Case IX as an example. The filtered compound B-mode image is displayed in Fig. 4(a) with a 30-dB dynamic range. Fig. 4(b) shows the extracted boundaries. The sound velocity distribution and attenuation coefficient distribution reconstructed using the algorithm introduced in Section 4 (with $c_{\text{lower}} = 1450$ m/s, $c_{\text{upper}} = 1580$ m/s, $f_0 =$ 5 MHz, $\Delta f =$ 4 MHz, $\alpha_{\text{dB,lower}} = 0$ dB/cm, and $\alpha_{\text{dB,upper}} = 10$ dB/cm) are shown in Fig. 4(c) and (d), respectively.

In all cases the estimation errors in the background regions are small. All the estimation results in the ROIs are plotted in Fig. 5. The reconstruction accuracy of the attenuation coefficient in the ROI was improved by applying the correction technique introduced in Section 3 except in Cases VII and VIII.

7. CONCLUDING REMARKS

In this study, we experimentally evaluated an approach for tomographic reconstructions of the sound velocity distribution and attenuation coefficient distribution in the breast using linear arrays. Nine cases were evaluated by scanning a phantom (made of materials mimicking different tissues in the breast) at different positions and the results demonstrate the feasibility of using a linear-array setup compatible with a B-mode imaging setup to estimate sound velocities and attenuation coefficients. With reference to Fig. 5, fat regions and tumors (including high-attenuation and irregular tumors) can be successfully discriminated by applying a threshold (e.g., 1500 m/s) to the sound velocities estimated in all relevant cases, and cysts and tumors can be successfully discriminated by applying another threshold (e.g., 3 dB/cm) to the estimated attenuation coefficients. Therefore, to improve the detection of breast cancer, B-mode image, sound velocity distribution, and attenuation coefficient distribution can be applied sequentially. *In vivo* experiments are underway to investigate the performance of this approach in clinical situations.

8. REFERENCES

[1] S. A. Goss, R. L. Johnston, and F. Dunn, "Compilation of empirical ultrasonic properties of mammalian tissues. II," *J. Acoust. Soc. Amer.*, vol. 68, no. 1, pp. 93–108, 1980.

[2] E. L. Madsen, E. Kelly-Fry, and G. R. Frank, "Anthropomorphic phantoms for assessing systems used in ultrasound imaging of the compressed breast," *Ultrasound Med. Biol.*, vol. 14, sup. 1, pp. 183–201, 1988.

[3] A. C. Kak and M. Slaney, *Principles of Computerized Tomographic Imaging*. New York: Institute of Electrical and Electronics Engineers, 1988.

[4] P. L. Combettes and P. Bondon, "Hard-constrained inconsistent signal feasibility problems," *IEEE Trans. Signal Processing*, vol. 47, no. 9, pp. 2460–2468, 1999.

[5] J. W. Goodman, *Introduction to Fourier Optics*. 2nd ed. New York: McGraw-Hill, 1996.

[6] S.-W. Huang and P.-C. Li, "Experimental investigation of computed tomography sound velocity reconstruction using incomplete data," *IEEE Trans. Ultrason., Ferroelect., Freq. Contr.*, vol. 51, no. 9, pp. 1072–1081, 2004.

[7] R. M. Lemor, P. K. Weber, P. K. Fonfara, C. Guenther, H. J. Welsch, and M. L. Hoss, "A new combined open research platform for ultrasound radio frequency signal processing," in *Proc. IEEE Ultrason. Symp.*, 2003, pp. 33–37.